The nature of oxygen states on the surfaces of CeO_2 and La–doped CeO_2

Patrick R. L. Keating [a] David O. Scanlon [b,c]
Graeme W. Watson *,[a]

[a] *Shcool of Chemistry and CRANN, Trinity College Dublin, Dublin 2, Ireland*

[b] *University College London, Kathleen Lonsdale Materials Chemistry, 20 Gordon Street, London WC1H 0AJ, United Kingdom*

[c] *Diamond Light Source Ltd., Diamond House, Harwell Science and Innovation Campus, Didcot, Oxfordshire OX11 0DE, United Kingdom*

Abstract

The oxygen states on CeO_2 surfaces were investigated with DFT+U calculations. The results reveal the variable nature of the oxygen states, including the never before modelled intrinsic peroxide surface defect. Under O–rich conditions, the peroxide defects on the (100) and (110) surfaces is more stable than oxygen vacancies. On surfaces doped with La(III) it is found that under O–rich conditions the (100) and (110) surface will preferentially form peroxide ions in response to the presence of the dopants while the (111) surface prefers oxygen vacancies. Calculated shifts in core levels match experimental binding energies, further suggesting the presence of peroxide species.

Key words: Ceria, Peroxide, Surfaces, Catalysis, Density Functional Theory, Doping
PACS:

1 Introduction

CeO_2 is a valuable material for a range of catalytic applications, such as three–way–catalysts (TWC) for automotive emissions,[1] water–gas–shift reactions,

* To whom correspondence should be addressed
Email addresses: keatinpr@tcd.ie (Patrick R. L. Keating), scanlond@gmail.com (David O. Scanlon), watsong@tcd.ie (Graeme W. Watson).

[2–4] and soot oxidation.[5,6] The effectiveness of CeO_2 as a catalyst is associated with its high oxygen storage capacity (OSC), i.e. the ability to absorb/release oxygen under oxidizing/reducing conditions,[7–10] and is related to the comparatively facile formation of O vacancies in CeO_2.[11,12] As an example of this simultaneous catalysis, CeO_2 can release oxygen, thus facilitating the oxidation of CO to CO_2, before reabsorbing it, which aids in the reduction of NO_2/NO to NO/N_2.[13]

Two common methods used to enhance the performance of CeO_2 catalysts are optimization of the synthesis and the addition of aliovalent dopants. The first method can enhance catalytic properties by altering the structure of the material, exposing the more reactive surfaces. The presence of dopants can improve CeO_2–based catalysts in several ways, for example by creating under–coordinated O anions, thus increasing the OSC,[14] or by increasing the number of catalytically active sites on the surface.[5]

The most commonly studied defect on CeO_2 surfaces is the O vacancy, due to its importance for describing catalysis of CeO_2.[15–18] Upon the formation of a neutral O vacancy, excess electrons are localized onto Ce(IV) ions, reducing them to Ce(III). In Kröger–Vink notation this is given as:

$$\mathrm{O}_\mathrm{O}^x + 2\mathrm{Ce}_\mathrm{Ce}^x \rightarrow V_\mathrm{O}^{\bullet\bullet} + 2\mathrm{Ce}'_\mathrm{Ce} + \frac{1}{2}\mathrm{O}_2 \tag{1}$$

where O_O^x and $\mathrm{Ce}_\mathrm{Ce}^x$ are an O^{2-} and a Ce^{4+} ion on their respective lattice sites. $V_\mathrm{O}^{\bullet\bullet}$ represents a neutral oxygen vacancy with an effective charge of 2+ at a O lattice site and Ce'_Ce is a Ce(III) ion at a Ce lattice site with an effective charge of -1. While it is generally agreed that Equation 1 represents the reduction mechanism for CeO_2, there is still little agreement about the exact structure of the reduced surfaces. The position of the Ce(III) ions relative to the vacancy has been extensively explored and several differing structures appear in the literature.[17,15] Although these varying cerium positions around the O vacancy have been explored on CeO_2, alternative oxygen states have yet to receive the same attention. Several studies have investigated and confirmed the presence of peroxide species on CeO_2 surfaces, but these have been solely related to adsorbed molecular oxygen.[19,40] For the bulk structure of CeO_2, peroxide ions have been demonstrated to be the most stable defect under oxygen rich conditions,[20] therefore the possibility exists that these defects may form intrinsically on the surfaces. The presence of such a competing defect could have a significant impact on our understanding of the catalytic properties of CeO_2.

A mechanism for enhancing the catalytic ability of CeO_2 is the introduction of dopant ions. Trivalent rare–earth cations have been shown to be effective for catalysis,[21] with La(III) being a promising candidate dopant.[6] It is generally considered that when CeO_2 is doped with a trivalent cation, such as La(III), two lattice Ce(IV) ions are replaced by the dopants and an O ion is

removed to conserve the charge.[22,23] In Kröger–Vink notation, this is:

$$O_O^x + 2Ce_{Ce}^x + La_2O_3 \rightarrow V_O^{\bullet\bullet} + 2La_{Ce}' + 2CeO_2 \quad (2)$$

where La_{Ce}' is a La(III) ion at a Ce lattice site with an effective charge of 1-. However, this mechanism was questioned by Fleming *et al.* who reported peaks in O 1*s* XPS data for La–doped CeO_2 that could not be explained by the formation of O vacancies.[24] Theoretical studies by Yeriskin and Nolan postulated that the defects were caused by O holes, which compensated the charge associated with the La dopants instead of the charge being compensated by removing an O anion.[25,26] The Kröger–Vink equation for this scheme is:

$$O_O^x + 2Ce_{Ce}^x + La_2O_3 \rightarrow 2O_O^{\bullet} + 2La_{Ce}' + 2CeO_2. \quad (3)$$

where $O_O^{\bullet}$ is a O hole on a O anion lattice site. To gain a full understanding of catalysis on CeO_2, it is necessary to fully explore all possible oxygen states and their chemical potential dependence. The interaction of adsorbing molecules with the surfaces of CeO_2 is dependent upon the defect chemistry and if there are flaws in the theoretical model the results may not be relevant.

In this report DFT+U calculations are employed to investigate the low index surfaces of CeO_2. On the reduced pure surfaces we observe a novel defect structure, based on the peroxide ion, that on some surfaces is thermodynamically more stable than intrinsic O vacancies. Similar results are also found on the La–doped surface where in certain cases peroxide ions can offer new, more stable structures to compensate the charge difference associated with the presence of the La(III) dopants. These differing oxygen states can potentially provide different reaction pathways, and hence could be of significant importance for understanding catalytic processes on the surfaces of CeO_2. Although a recent theoretical study did discuss the presence of peroxy and superoxy species on CeO_2,[27] so far such defects have only been described for the undoped (110) and (111) surfaces.

2 Theoretical Methods

Total energy calculations were carried out in a plane wave basis set (400 eV cut off) with the Perdew–Burke–Ernzerhof (PBE) functional[28] as implemented in the VASP code.[29–31] To model localized electronic states, a +U correction was applied to the Ce 4*f* states (U=5.0 eV) and the O 2*p* states (U=5.5 eV).[20] The interaction between the core and valence states were modeled with the projector augmented wave (PAW) method.[32]. The surfaces were constructed from the CeO_2 unit cell with the METADISE program.[33] The surfaces were modelled with the slab method with a vacuum gap of 15 Å between the surfaces of each slab. The simulations cells employed were; a

(2×2) expansion with a slab thickness of 13.10 Å (120 atoms, 11 atomic layers) for the (100) surface; a (2×3) expansion with a slab thickness of 11.55 Å (126 atoms, 7 atomic layers) for the (110) surface; and a (4×4) expansion with a slab thickness of 14.16 Å (240 atoms, 15 atomic layers) for the (111) surface. All surfaces were simulated using a 1×1×1 Monkhorst–Pack k–point grid[34], and calculations were deemed converged when the forces on each ion where $< 0.01\,\mathrm{eV/Å}$. The defect formation energies were calculated according to the equation $\Delta H_\mathrm{f}(\mathrm{D}) = (E^\mathrm{D} - E^\mathrm{H}) + \sum_i n_i(E_i + \mu_i)$ where E^H is the total energy of the host supercell and $E^{(\mathrm{D})}$ is the energy of the defect cell. E_i are the elemental energies, i.e. the energies of the constituent elements in their standard states (e.g. Ce(s) and O_2(g)) and n is the number of atoms of a element added to (positive) or taken from (negative) an external reservoir. μ_i are the chemical potentials of the elements and are to used to approximate the formation of defects under different growth conditions. The upper limit for the chemical potentials (O–rich) was set as the formation of O_2(g) while the lower limit (O–poor) was set by the formation of Ce_2O_3 and La_2O_3.[35] To aid in the modelling of localised defects, the occupation matrix method was employed,[36] which allows the relaxation of a structure with constrained electrons/holes, allowing a polaron distortion to form at the required position. Once the defects were localised, the occupation matrix was removed and the structure allowed to relax. The vibrational frequencies for the peroxide ions were determined by shifting the position of the oxygens in the peroxide ion and then numerically calculating the 2$^{\mathrm{nd}}$ derivative of the forces on the atoms while holding the rest of the structure constant. PBE is well known to overestimate the bond length, and hence underestimate the vibrational frequencies. For example, the calculated O_2 bond length was 1.23 Å, compared to the experimental value of 1.21 Å.[37] Therefore, the frequencies were corrected by the error between the calculated O–O stretching frequency of the O_2(g) molecule ($1500\,\mathrm{cm^{-1}}$) and the experimental value ($1556\,\mathrm{cm^{-1}}$).[38]

3 Results

For the three low index surfaces, (100), (110) and (111), two neutral defect clusters were studied; an O vacancy with two Ce(III) ions ($[\mathrm{Ce}'_\mathrm{Ce}$–$V_\mathrm{O}^{\bullet\bullet}$–$\mathrm{Ce}'_\mathrm{Ce}]$) and the previously unstudied structure where two Ce(III) ions with a peroxide ion replacing two lattice O ions ($[\mathrm{Ce}'_\mathrm{Ce}$–$(\mathrm{O}_2)''_i$+$2V_\mathrm{O}^{\bullet\bullet}$–$\mathrm{Ce}'_\mathrm{Ce}]$). O holes were also tested on the surfaces, i.e. $[\mathrm{Ce}'_\mathrm{Ce}$–$\mathrm{O}^{\bullet}_\mathrm{O}]$, but in all cases it was found that the electron on the Ce(III) ion would spontaneously quench the O hole. A wide range of different configurations were tested for the two defects by varying the position of the Ce(III) ions and the O vacancy/peroxide ion to determine the most stable structure. The formation energies for the most stable configuration of intrinsic surface defects are summarized in Table 1. We can see that under

Table 1
The chemical potential dependent defect formation energies for the low index surfaces of CeO_2. All energies are given in eV.

	(100)		(110)		(111)	
	O–poor	O–rich	O–poor	O–rich	O–poor	O–rich
$[Ce'_{Ce}$– $V_O^{\bullet\bullet}$–$Ce'_{Ce}]$	-0.89	0.75	-1.12	0.52	-0.60	1.04
$[Ce'_{Ce}$–$(O_2)''_i$+$2V_O^{\bullet\bullet}$–$Ce'_{Ce}]$	0.35	0.35	0.30	0.30	1.14	1.14

both O–rich and O–poor conditions, the O vacancy is the favored defect for the (111) surface. However, on the (100) and (110) surfaces the peroxide defect is the most stable under O–rich conditions.

The lowest energy vacancy and peroxide defects for each surface are shown in Figure 1. For the vacancy defects (Figure 1 (a)–(c)), the position of the vacancy and its distance from the Ce(III) ions are in agreement with previous studies of the (100),[16] (110)[15] and (111)[39] surfaces. For the peroxide defects, two neighboring O ions move from their lattice positions to an interstitial site and form a peroxide anion, $(O_2)''_i$ (Figure 1 (d)–(f)), while two neighboring Ce(IV) ions are reduced to Ce(III). On the (100) surface two O ions move 1.91 Å from their lattice sites; on the (110) surface two O ions move 0.74 Å from their lattice positions; and on the (111) surface, a sub–surface O ion and a surface O ion move 0.64 Å and 0.90 Å, respectively, from their lattice sites. The resulting O–O bond lengths are 1.50 Å (100), 1.53 Å (110) and 1.53 Å (111), all of which are characteristic of a peroxide species.[37]

The calculated vibrational frequencies of the O–O stretch in the intrinsic peroxide ion were 864 cm^{-1}, 802 cm^{-1} and 834 cm^{-1} on the (100), (110) and the (111) surfaces respectively. In previous spectroscopic studies of CeO_2 surfaces, peaks at ∼877–831 cm^{-1} in the Raman spectra were assigned to O–O stretching of peroxide species from adsorbed O_2 molecules.[40,19] Wu *et al.* observed peaks at 840 cm^{-1} and 863 cm^{-1} in the Raman spectra of nanorods, which express the (100) and (110) surfaces, and and a peak at 840 cm^{-1} in the spectra of nanocubes, which only expose the (100) surface. In contrast, extremely weak peaks at these frequencies were seen for nano-octahedra, whose surfaces are exclusively (111) in nature. The results presented in this paper demonstrate that intrinsic peroxide defects readily form on the (100) surface, and the vibrational frequencies match experimentally determined values, indicating that the peaks observed may be from intrinsic peroxide ions and not due to adsorbed species. Furthermore, the lack of peaks for the (111) surfaces is in agreement with the energetic data presented in Table 1, which shows that the peroxide ion is never stable on the (111) surface. The calculated peroxide vibration frequency on the (110) surface (802 cm^{-1}) does not match the experimental value (863 cm^{-1}). However, the experimental peaks associated with (110) surfaces were higher in frequency than those of the (100) surfaces,

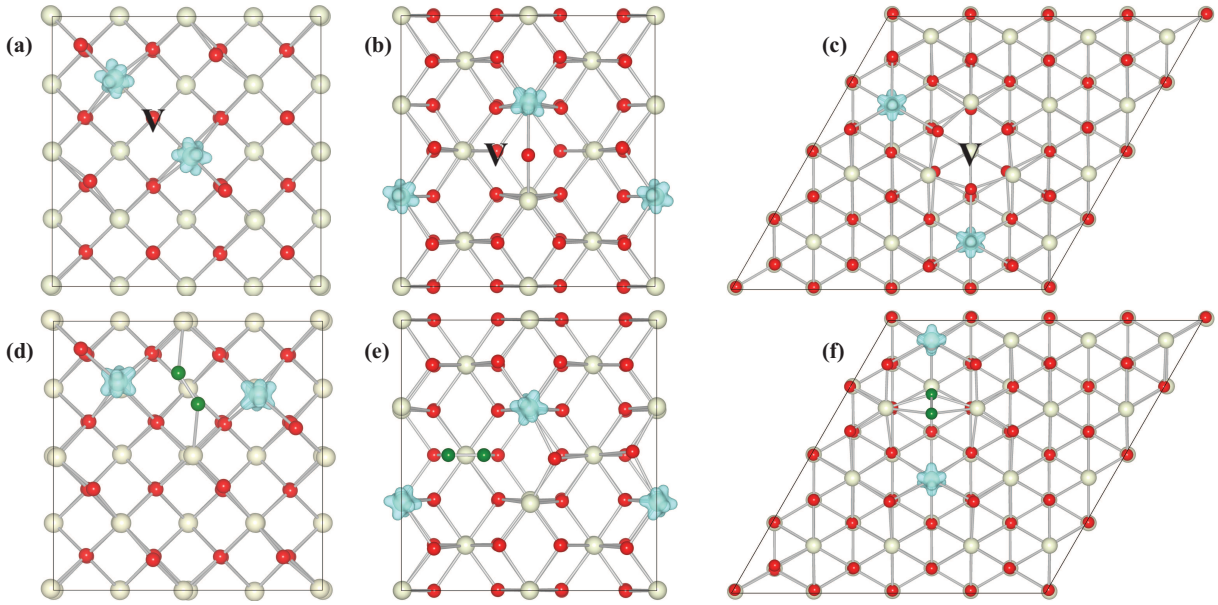

Fig. 1. The low index surfaces of CeO_2 displaying the structures and spin density plots of the O vacancy defect on the (a) (100), (b) (110) and (c) (111) surfaces and the peroxide ion defect on the (d) (100), (e) (110) and (f) (111) surfaces. The Ce and O ions are represented by the white and red spheres respectively. The position of the vacancy is denoted by the letter V. The peroxide ion is represented by the dark green spheres. The isosurfaces, displaying the excess spin electrons on the cerium ions, are shown in blue and are set to $0.05\,e/Å^3$

which Wu *et al.* claimed was a result of the defects forming clusters on the (110) surface, whereas they remained isolated on the (100). Since only isolated defects were calculated, this could account for the disparity between the experimental and calculated frequencies. The possibility of the intrinsic surface peroxide species being present in reduced CeO_2 at high oxygen partial pressures may be significant for understanding CeO_2 catalysis, as previous studies have only considered reactions through the O vacancy[17,13,41] or through adsorbed peroxo/superoxo species.[42,43,40]

Having demonstrated that alternative oxygen states to the O vacancy are valid defect structures on reduced pure CeO_2 surfaces, the La–doped CeO_2 surfaces were also investigated to examine whether these peroxide species are a viable mechanism for charge compensation. Several types of charge compensation for the dopants were tested for each surface: one lanthanum dopant compensated by one oxygen hole ($[La'_{Ce}+O^{\bullet}_{O}]$); two lanthanum dopants compensated by two oxygen holes ($[2La'_{Ce}+2O^{\bullet}_{O}]$); two lanthanum dopants compensated by a peroxide ion formed from lattice O ions ($[2La'_{Ce}+(O_2)''_i+2V^{\bullet\bullet}_{O}]$); and finally two lanthanum dopants charge compensated by an O vacancy ($[2La'_{Ce}+V^{\bullet\bullet}_{O}]$). For each defect, several different configurations were investigated by varying the distance between the dopant cations and the charge compensating defects to determine the most stable structure for each system. The doping energies

Table 2
The chemical potential dependent doping energies for different compensation mechanisms on the low index surfaces of CeO_2. The energy of the $[La'_{Ce}+O^{\bullet}_{O}]$ defect has been multiplied by 2 so as to match the stoichiometry of the other defects. All energies are given in eV.

Defect	O–poor			O–rich		
	100	110	111	100	110	111
$[La'_{Ce}+O^{\bullet}_{O}]$ ($\times$ 2)	0.40	0.58	1.38	-1.24	-1.04	-0.26
$[2La'_{Ce}+ 2\ O^{\bullet}_{O}]$	0.44	0.54	1.29	-1.19	-1.09	-0.34
$[2La'_{Ce}+(O_2)''_i+2V^{\bullet\bullet}_{O}]$	0.14	0.30	1.00	-1.50	-1.34	-0.64
$[2La'_{Ce}+V^{\bullet\bullet}_{O}]$	-1.10	-1.28	-0.70	-1.10	-1.28	-0.70

for most stable defect of each type are shown in Table 2.

Under O–poor conditions, the O vacancy is the preferred compensation mechanism on all surfaces, with doping energies of -1.01 eV, -1.28 eV and -0.70 eV for the (100), (110) and (111) surfaces respectively. At the O–rich limit, however, the preferred compensation mechanism on the (100) and (110) surfaces is now a peroxide ion, with doping energies of -1.50 eV for the (100) surface and -1.34 eV on the (110) surface. Vacancy compensation is still more stable for the (111) surface, with a doping energy of -0.70 eV compared to -0.64 eV for the peroxide ion. Charge compensation through O holes was found to be unstable under O–poor conditions, but is significantly stabilised under O–rich conditions, and for the (100) surface it is the second most stable compensation mechanism after peroxide compensation. It is worth noting that the doping energy for two isolated holes on the (100) surface was lower than for two clustered holes, i.e. $[La'_{Ce}+O^{\bullet}_{O}] \times 2$ is more stable than $[2La'_{Ce}+ 2\ O^{\bullet}_{O}]$, suggesting that it is unfavourable for La(III) ions to cluster on the (100) surface.

An x–ray photoelecton spectroscopy (XPS) study by Fleming *et al.*[24] investigated La–doped CeO_2 nanocrystals, which predominantly express the (111) surface but also have significant contributions from the (110) and the (111) surfaces. They discovered a peak in the O 1*s* spectra displaying a binding energy 1.5–1.8 eV higher than the average O 1*s* contributions. In contrast to the results presented in this letter, they suggested it may be due to a charge compensating mechanism featuring O holes. To compare to the XPS data, the shift in O 1*s* core levels between O holes/peroxide and surface O anions was calculated. The O 1*s* core level shifts for both hole states and peroxide ions are shown in Table 3. It was found that these 1*s* core levels were lower in energy than the average of the other surface O 1*s* core levels, which would correspond to the higher binding energies observed experimentally. For O holes, the shift in core level energies only matches that which was observed by Fleming *et al.* for holes on the (111) surface, however, the energetic data suggests that

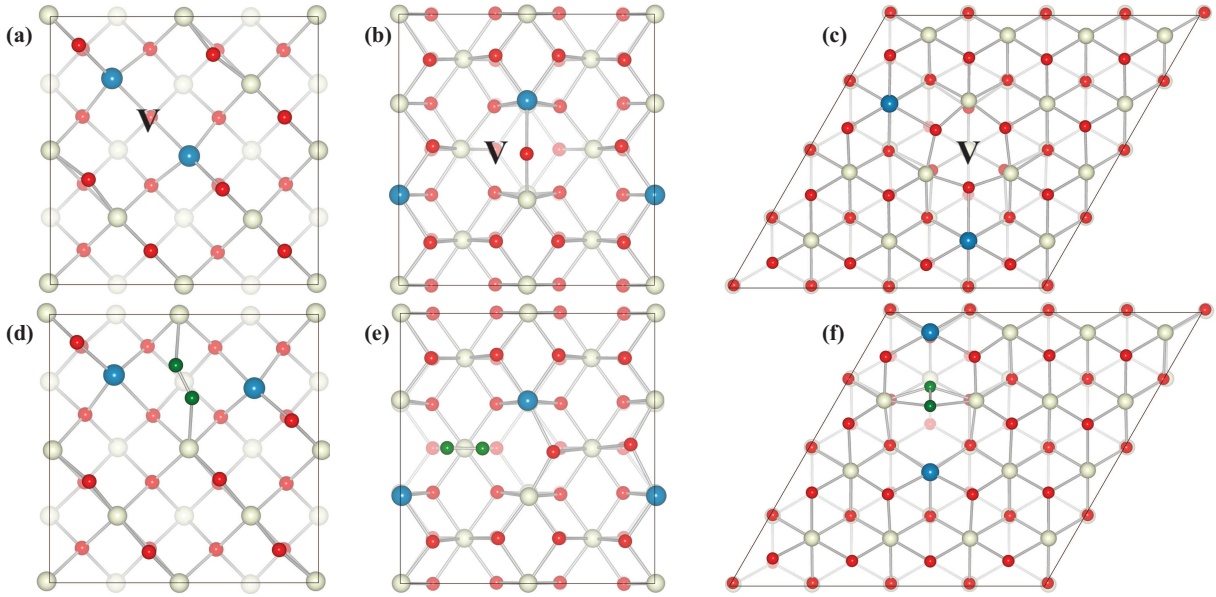

Fig. 2. The low index surfaces of CeO_2 displaying the [La'_{Ce}–$V_O^{\bullet\bullet}$–La'_{Ce}] defect on the (a) (100), (b) (110) and (c) (111) surfaces and the [La'_{Ce}–$(O_2)''_i$+$2V_O^{\bullet\bullet}$–La'_{Ce}] defect on the (d) (100), (e) (110) and (f) (111) surfaces. The position of the O vacancy is denoted by the letter V. The La(III) ions are represented by the dark blue spheres.

Table 3
The shift in core level energies for O holes and peroxide ions compared to O^{2-} anions on the La–doped low index surfaces of CeO_2. All energies are given in eV.

	(100)	(110)	(111)
$O_O^{\bullet}$	-1.43	-1.18	-1.53
$(O_2)''_i$	-1.67	-1.73	-2.22

such defects are not stable on the (111) surface. For the peroxide ions on the surfaces, the shifts in core level energies on the (100) and (110) surface are within the experimentally observed range, and hence the peaks observed by Fleming *et al.* are likely to be due to a peroxide compensation mechanism, and not O holes. Peaks corresponding to the calculated peroxide shift on the (111) surface was not seen, but their absence is understandable given that under all conditions, the O vacancy is the most stable charge compensation scheme on the (111) surface.

4 Conclusions

This letter demonstrates that the nature of the oxygen states on the low index surfaces of pure and La–doped CeO_2 play a vital role in the surface chemistry of these materials. Under O–rich conditions, the formation of a previously unobserved peroxide ion is more stable than an O vacancy on the (100) and

(110) surfaces. Similarly, for La–doped (100) and (110) surfaces under O–rich conditions, the preferred method of charge compensation is the peroxide ion as opposed to the traditional $[2La'_{Ce}–V_O^{\bullet\bullet}]$ defect cluster. The formation of peroxide defects is also consistent with Raman spectra of the pure surfaces and core level shifts observed in La–doped CeO_2. These defects may also help to explain the results of experimental studies by supporting evidence for new reaction pathways and expanding the knowledge of the role CeO_2 plays in heterogeneous catalysis.

Acknowledgements

This work was supported by Science Foundation Ireland through the Research Frontiers Programme (grant numbers 08/RFP/MTR1044 and 09/RFP/MTR2274) and by COST Action CM1104. Calculations were performed on the Lonsdale supercomputer as maintained by TCHPC, and the Stokes supercomputer as maintained by ICHEC.

References

[1] S. Y. Christou, A. M. Efstathiou, Efficient in–situ regeneration method of the catalytic activity of aged TWC, Top. Catal. 42–43 (2007) 415–419.

[2] W. L. Deng, C. Carpenter, N. Yi, M. Flytzani-Stephanopoulos, Comparison of the activity of Au/CeO_2 and Au/Fe_2O_3 catalysts for the CO oxidation and the water–gas shift reactions, Top. Catal. 44 (2007) 199–208.

[3] R. Si, M. Flytsani-Stephanopoulos, Shape and crystal–plane effects of nanoscale ceria on the activity of Au–CeO_2 catalysts for the water–gas shift reaction, Angew. Chem., Int. Ed. 47 (2008) 2884–2887.

[4] P. Panagiotopoulou, J. Papavasiliou, G. Avgouropoulos, T. Ioannides, Water–gas shift activity of doped Pt/CeO_2 catalysts, Chem. Eng. J. 134 (2007) 16–22.

[5] E. Aneggi, C. de Leitenburg, G. Dolcetti, A. Trovarelli, Promotional effect of rare earths and transition metals in the combustion of diesel soot over CeO_2 and CeO_2-ZrO_2, Catal. Today 114 (2006) 40–47.

[6] K. Krishna, A. Bueno-Lopez, M. Makkee, J. A. Moulijn, Potential rare–earth modified CeO_2 catalysts for soot oxidation, Top. Catal. 42–43 (2007) 221–228.

[7] N. V. Skorodumova, S. I. Simak, B. I. Lundqvist, I. A. Abrikosov, B. Johansson, Quantum origin of the oxygen storage capability of ceria, Phys. Rev. Lett. 89 (2002) 166601.

[8] Z. X. Yang, T. K. Woo, K. Hermansson, Adsorption of NO on unreduced and reduced CeO_2 surfaces: A plane–wave DFT study, Surf. Sci. 600 (2006) 4953–4960.

[9] D. O. Scanlon, N. M. Galea, B. J. Morgan, G. W. Watson, Reactivity on the (110) surface of ceria: A GGA plus U study of surface reduction and the adsorption of CO and NO_2, J. Phys. Chem. C 113 (2009) 11095–11103.

[10] M. Nolan, J. E. Fearon, G. W. Watson, Oxygen vacancy formation and migration in ceria, Solid State Ionics 177 (2006) 3069–3074.

[11] E. B. Lavik, I. Kosacki, H. L. Tuller, Y. M. Chiang, J. Y. Ying, Nonstoichiometry and electrical conductivity of nanocrystalline Ceo_{2-x}, J. Electroceram. 1 (1997) 7–14.

[12] P. R. L. Keating, D. O. Scanlon, G. W. Watson, Intrinsic ferromagnetism in Ceo_2: dispelling the myth of vacancy site localization mediated superexchange, J. Phys.: Condens. Matter 21 (2009) 405502.

[13] M. Nolan, S. C. Parker, G. W. Watson, CeO_2 catalysed conversion of CO, NO_2 and NO from first principles energetics, Phys. Chem. Chem. Phys. 8 (2006) 216–218.

[14] A. B. Kehoe, D. O. Scanlon, G. W. Watson, Role of lattice distortions in the oxygen storage capacity of divalently doped CeO_2, Chem. Mater. 23 (2011) 4464–4468.

[15] J. Kullgren, K. Hermansson, C. Castleton, Many competing ceria (110) oxygen vacancy structures: From small to large supercells, J. Chem. Phys. 137 (2012) 044705.

[16] M. Nolan, S. Grigoleit, D. C. Sayle, S. C. Parker, G. W. Watson, Density functional theory studies of the structure and electronic structure of pure and defective low index surfaces of ceria, Surf. Sci. 576 (2005) 217–229.

[17] N. M. Galea, D. O. Scanlon, B. J. Morgan, G. W. Watson, A GGA+U study of the reduction of ceria surfaces and their partial reoxidation through NO_2 adsorption, Mol. Simul. 35 (2009) 577–583.

[18] C. J. Zhang, A. Michaelides, D. A. King, S. J. Jenkins, Oxygen vacancy clusters on ceria: Decisive role of cerium f electrons, Phys. Rev. B 79 (2009) 075433.

[19] Z. L. Wu, M. J. Li, J. Howe, H. M. Meyer, S. H. Overbury, Probing defect sites on CeO_2 nanocrystals with well–defined surface planes by Raman spectroscopy and O_2 adsorption, Langmuir 26 (2010) 16595–16606.

[20] P. R. L. Keating, D. O. Scanlon, B. J. Morgan, N. M. Galea, G. W. Watson, Analysis of intrinsic defects in CeO_2 using a Koopmans-like GGA+U approach, J. Phys. Chem. C 116 (2012) 2443–2452.

[21] W. Y. Hernandez, M. A. Centeno, F. Romero-Sarria, J. A. Odriozola, Synthesis and characterization of $Ce_{1-x}Eu_xO_{2-x/2}$ mixed oxides and their catalytic activities for CO oxidation, J. Phys. Chem. C 113 (2009) 5629–5635.

[22] H. Hayashi, R. Sagawa, R. Inaba, K. Kawamura, Molecular dynamics calculations on ceria–based solid electrolytes with different radius dopants, Solid State Ionics 131 (2000) 281–290.

[23] D. A. Andersson, S. I. Simak, N. V. Skorodumova, I. A. Abrikosov, B. Johansson, Optimization of ionic conductivity in doped ceria, Proc. Natl. Acad. Sci. U.S.A. 103 (2006) 3518–3521.

[24] P. Fleming, S. Ramirz, J. D. Holmes, M. A. Morris, An XPS study of the oxidation of reduced ceria-lanthana nanocrystals, Chem. Phys. Lett. 501 (2011) 51–57.

[25] I. Yeriskin, M. Nolan, Effect of La doping on CO adsorption at ceria surfaces, J. Chem. Phys. 131 (2009) 244701.

[26] I. Yeriskin, M. Nolan, Doping of ceria surfaces with lanthanum: a DFT+U study, J. Phys.: Condens. Matter 22 (2010) 135004.

[27] J. Kullgren, K. Hermansson, P. Broqvist, Reactive oxygen species in stoichiometric ceria: Bulk and low–index surfaces, Phys. Status Solidi RRL (2014) 10.1002/pssr.201409099.

[28] J. P. Perdew, K. Burke, M. Ernserhof, Generalized gradient approximation made simple, Phys. Rev. Lett. 77 (1996) 3865–3868.

[29] G. Kresse, J. Hafner, *Ab–initio* molecular–dynamics simulation of the liquid–metal amorphous–semiconductor transition in germanium, Phys. Rev. B 49 (1994) 14251–14269.

[30] G. Kresse, J. Furthmüller, Efficient iterative schemes for *Ab–initio* total–energy calculations using a plane–wave basis set, Phys. Rev. B 54 (1996) 11169–11186.

[31] G. Kresse, J. Furthmüller, Efficiency of *Ab–initio* total energy calculations for metals and semiconductors using a plane–wave basis set, Comput. Mater. Sci. 6 (1996) 12–50.

[32] P. E. Blöchl, Projector augmented–wave method, Phys. Rev. B 50 (1994) 17953–17979.

[33] G. W. Watson, E. T. Kelsey, N. H. de Leeuw, D. J. Harris, S. C. Parker, Atomistic simulation of dislocations, surfaces and interfaces in MgO, J. Chem. Soc., Faraday Transactions 92 (1996) 433–438.

[34] H. J. Monkhorst, J. D. Pack, Special points for Brillouin–zone integrations, Phys. Rev. B 13 (1976) 5188–5192.

[35] P. R. L. Keating, D. O. Scanlon, G. W. Watson, Computational testing of trivalent dopant in ceo_2 for improved high–κ dielectric behaviour, J. Mater. Chem. C 1 (2013) 1093–1098.

[36] J. P. Allen, G. W. Watson, Occupation matrix control of d and f electron localisation using dft+U, Phys. Chem. Chem. Phys. (2014) 10.1039/c4cp01083c.

[37] A. F. Holleman, E. Wiber, N. Wiberg, Inorganic Chemistry, Academic Press, San Diego, CA, USA, 2001.

[38] A. Weber, E. A. McGinnis, The raman spectrum of gaseous oxygen, J. Mol. Spectry. 4 (1960) 195–200.

[39] H. F. Wang, H. Y. Li, X. Q. Gong, Y. L. Guo, G. Z. Lu, P. Hu, Oxygen vacancy formation in CeO_2 and $Ce_{1-x}Zr_xo_2$ solid solutions: Electron localization, electrostatic potential and structural relaxation, Phys. Chem. Chem. Phys. 14 (2012) 16521–16535.

[40] V. V. Pushkarev, V. I. Kovalchuk, J. L. d'Itri, Probing defect sites on the CeO_2 surface with dioxygen, J. Phys. Chem. B 108 (2004) 5341–5348.

[41] N. Shehata, K. Meehan, M. Hudait, N. Jain, Control of oxygen vacancies and Ce^{+3} concentrations in doped ceria nanoparticles via the selection of lanthanide element, J. Nanopart. Res. 14 (2012) 1173.

[42] X. N. Wu, X. L. Ding, S. M. Bai, B. Xu, S. G. He, Q. Shi, Experimental and theorectical study of the reactions between cerium oxide cleanusteclanions and carbon monoxide: Size–dependent reactivity of the Ce_nO_{2n+1} - (n=1–21), J. Phys. Chem. C 115 (2011) 13329–13337.

[43] M. Huang, S. Fabris, Role of surface peroxo and superoxo species in the low–temperature oxygen buffering of ceria: Density functional theory calculations, Phys. Rev. B 75 (2007) 081404.